Imaging Lipid Synthesis in Hepatocellular Carcinoma with [Methyl-^{11}C]Choline: Correlation with In Vivo Metabolic Studies

Yu Kuang*[1], Nicolas Salem*[1], Haibin Tian[2], Jeffrey A. Kolthammer[1], David J. Corn[2], Chunying Wu[2], Fangjing Wang[1], Yanming Wang[2], and Zhenghong Lee[1,2]

[1]*Department of Biomedical Engineering, Case Western Reserve University, Cleveland, Ohio; and* [2]*Nuclear Medicine Division, Department of Radiology, University Hospitals Case Medical Center, Cleveland, Ohio*

PET with [methyl-^{11}C]-choline (^{11}C-choline) can be useful for detecting well-differentiated hepatocellular carcinoma (HCC) that is not ^{18}F-FDG–avid. This study was designed to examine the relationship between choline metabolism and choline tracer uptake in HCC for PET with ^{11}C-choline. **Methods:** Dynamic PET scans of ^{11}C-choline were acquired using the woodchuck models of HCC. After imaging, [methyl-^{14}C]-choline was injected, and metabolites from both HCC tissue samples and the surrounding hepatic tissues were extracted and analyzed by radio–high-performance liquid chromatography. The enzymatic activities of choline kinase and choline-phosphate cytidylyltransferase were assayed for correlation with the imaging and metabolism data. **Results:** PET with ^{11}C-choline showed an HCC detection rate of 9 of 10. The tumor-to-liver ratio for the 9 detected HCCs was 1.89 ± 0.55. Hematoxylin-eosin staining confirmed that all spots with high tracer uptake were well-differentiated HCCs. Variation of radioactivity distribution within HCCs indicated a heterogeneous uptake of choline. The activities of both choline kinase and choline-phosphate cytidylyltransferase were found to be significantly higher in HCC than in the surrounding hepatic tissues. The major metabolites of ^{11}C-choline were phosphocholine in HCC and betaine and choline in the surrounding hepatic tissues at 12 min after injection; in HCC, phosphocholine rapidly converted to phosphatidylcholine at 30 min after injection. **Conclusion:** HCCs display enhanced uptake of radiolabeled choline despite a moderate degree of physiologic uptake in the surrounding hepatic tissues. Initially, increased radiolabeled choline uptake in HCCs is associated with the transport and phosphorylation of choline; as time passes, the increased uptake of radiolabeled choline reflects increased phosphatidylcholine synthesis derived from radiolabeled cytidine 5′-diphosphocholine (CDP-choline) in HCCs. In contrast, the surrounding hepatic tissues exhibit extensive oxidation of radiolabeled choline via the phosphatidylethanolamine methylation pathway, a major contributor to the observed physiologic uptake.

Key Words: PET of hepatocellular carcinoma; radiolabeled choline; CDP-choline pathway; phosphatidylethanolamine methylation pathway; choline-phosphate cytidylyltransferase

J Nucl Med 2011; 52:98–106
DOI: 10.2967/jnumed.110.080366

Hepatocellular carcinoma (HCC) is the fifth most common tumor and the third most common cause of cancer death worldwide. The survival of patients with HCC remains dismal (<3 mo) (*1*). In the United States, HCC has exhibited the largest increase in incidence over the last 10 y. This increase is caused, in part, by the epidemic of hepatitis B and C viral infections, which can lead to cirrhosis and HCC. The incidence and death rates are similar, indicating the overall poor survival of HCC. Detecting HCC in its early stages may provide patients with more opportunities for curative treatments and for prolonged survival.

PET using ^{18}F-FDG as a probe has been shown to be a powerful tool for detection, staging, and therapy monitoring for malignant tumors (*2*). However, ^{18}F-FDG does not show uptake in well-differentiated HCC, which is an early stage of primary liver cancer, leading to a high false-negative rate (*3*).

We previously reported the effectiveness of [methyl-^{11}C]-choline (^{11}C-choline) for imaging well-differentiated HCC (*4*). Despite a background uptake of radiolabeled choline in normal liver tissues, PET using ^{11}C-choline detected all HCCs with a tumor-to-liver (T/L) ratio of 1.63 ± 0.34 (*4*). Histopathologic evaluation revealed that these tumors were well-differentiated. In a clinical study, ^{18}F-fluorocholine also detected all HCCs with a T/L of 1.50 ± 0.38, with the maximum standardized uptake value higher in well-differentiated tumors (*5*).

The signal intensity observed in PET images originates from bolus-injected radiolabeled choline and its derivative radiolabeled metabolites. The metabolism of radiolabeled choline is also influenced by the microenvironment of tumors. Thus, various questions exist: What are the transient metabolites of radiolabeled choline? Which molecular

Received Jun. 18, 2010; revision accepted Sep. 23, 2010.
For correspondence or reprints contact: Zhenghong Lee, Nuclear Medicine Division, Department of Radiology, University Hospitals Case Medical Center, 11100 Euclid Ave., Cleveland, OH 44106.
E-mail: zhenghong.lee@case.edu
*Contributed equally to this work.

species are involved in the increased radiolabeled choline uptake in HCCs? How are these metabolite changes correlated with the interpretation of PET images? To elucidate the mechanism of tracer accumulation, we studied the metabolic fate of radiolabeled choline in the woodchuck model of HCC for correlation with PET using choline. ^{18}F-FDG also served as a clinical tracer for comparison in this study.

As shown in Supplemental Figure 1 (supplemental materials are available online only at http://jnm.snmjournals.org), there are 3 major potential metabolic pathways of injected ^{11}C-choline. After transportation into the cells by choline transporter, choline can be phosphorylated to phosphocholine by choline kinase. Phosphocholine can be converted to CDP-choline with the catalysis of cholinephosphate cytidylyltransferase, also known as CTP:phosphocholine cytidylyltransferase or CCT, and further incorporated into phosphatidylcholine in the CDP-choline pathway. In neuronal cells, choline can also be converted to acetylcholine. In the liver and kidney, choline can be oxidized to betaine, an osmolyte and a methyl group donor. As an organic osmolyte, betaine is accumulated or released by cells to maintain homeostasis of cell volume (*6*). Betaine can also provide the methyl group to methionine and subsequently produce s-adenosylmethionine, which can eventually incorporate into phosphatidylcholine through a reaction with phosphatidylethanolamine in the phosphatidylethanolamine methylation pathway. There is a profound distinction in phosphatidylcholine species between the CDP-choline pathway and the phosphatidylethanolamine methylation pathway (*7,8*). This distinction may contribute to the different functions of these 2 pathways in the liver.

We used the eastern woodchuck (*Marmota monax*) model of HCC induced by the woodchuck hepatitis virus (WHV) infection—an interesting animal model of human HCC (*9*)—in this study. WHV is a member of the family Hepadnaviridae, genus *Orthohepadnavirus*, of which human hepatitis B virus is the prototype. Like hepatitis B virus, WHV infects the liver and can cause acute and chronic hepatitis. Furthermore, chronic WHV infection in woodchucks usually leads to development of HCC within the first 2–4 y of life.

MATERIALS AND METHODS

Materials

All chemical reagents used were obtained from Sigma Chemicals unless otherwise stated. [Methyl-^{14}C]-choline chloride (^{14}C-choline; specific activity, 2.035 GBq/mmol) and [methyl-^{14}C]-phosphocholine (specific activity, 2.035 GBq/mmol) were obtained from American Radiochemical Inc. Organic solvents were purchased from Fisher Scientific.

Animals

All procedures in this study followed the guidelines of the Institutional Animal Care and Use Committee of Case Western Reserve University. WHV-carrier woodchucks (n = 10) were obtained from Northeastern Wildlife Inc. The weights of all animals were between 2.3 and 5 kg.

PET/CT

^{18}F-FDG and ^{11}C-choline images were acquired according to the procedures described previously (*4*). Before PET/CT, woodchucks were kept fasting overnight and were initially sedated with an intramuscular cocktail injection of xylazine (5 mg/kg) and ketamine (50 mg/kg) for anesthetic induction. The PET/CT scans were obtained using a Philips Gemini-TF PET/CT scanner. Each animal was intravenously injected with a bolus of 37 MBq of ^{11}C-choline and, in a different imaging session, ^{18}F-FDG. Dynamic emission scans were acquired for 60 min while the animals remained anesthetized using a 1:10 dilution of pentobarbital (Nembutal; Abbott Pharmaceutical) in saline solution. The list-mode data were rebinned, the row-action maximum likelihood algorithm was used to reconstruct the 3-dimensional emission scan data, and CT-based attenuation correction was used, yielding a voxel size of 4 × 4 × 4 mm.

Image Analysis

Analysis of the uptake of the radiopharmaceuticals in the primary tumors was performed using standardized uptake values from regions of interest defined on PET images. Circular regions of interest were manually drawn over the primary tumor and also over hepatic tissues surrounding the HCCs. The T/L ratio for each focus of uptake was also calculated. Time frames between 25 and 30 min were used to quantify the standardized uptake value and T/L. A tumor was deemed present if the T/L was greater than 1.2 (*4*).

Histology

Histologic evaluation was used for correlation with in vivo PET data. After PET/CT, a selection of animals was euthanized immediately using a barbiturate overdose (FatalPlus; Vortech Pharmaceuticals Inc.). For these woodchucks, samples of HCCs and the surrounding hepatic tissues were harvested postmortem and fixed in formalin. Thin sections of paraffin-embedded tissues were prepared and stained with hematoxylin and eosin (H&E) (*4*). Additional woodchuck HCC tissues were obtained from MRI-guided biopsy for H&E staining.

^{14}C-Choline Metabolism in Woodchuck Model of HCC

After PET/CT with ^{11}C-choline, a selection of woodchucks was used for in vivo metabolite analysis. Because of the short half-life of ^{11}C (20 min), ^{14}C-choline was used to characterize the different compositions of radiolabeled metabolites between HCCs and surrounding hepatic tissues. A bolus of 18.5 MBq of ^{14}C-choline was intravenously injected. The woodchucks were euthanized at 12 or 30 min after injection, and their livers were excised immediately. The tissue samples from HCC regions and surrounding hepatic tissues were harvested for the extraction of choline metabolites.

Extraction of Radiolabeled Metabolites

The extraction of radiolabeled metabolites from liver tissues followed the method of Folch et al. (*10*). The tissue homogenate was separated into a liquid phase (water-soluble phase and lipid-soluble phase) and an insoluble phase. The metabolites in the water-soluble and lipid-soluble phases were analyzed using high-performance liquid chromatography (HPLC) as described in the "Analysis of Radiolabeled Metabolites" section. The insoluble phase was further separated into RNA hydrolysate, DNA hydrolysate, and protein fractions as reported previously (*11*). The ^{14}C-choline incorporated into lipid-soluble, water-soluble, RNA hydrolysates, DNA hydrolysates, and protein fractions were counted with an LS-6500 liquid scintillation counter (Beckman

Coulter Inc.) using Bio-Safe II scintillation fluid (Fisher Scientific). The radioactivity in each of the metabolites was normalized to total tissue protein content using a Bradford kit (Bio-Rad Laboratories, Inc.).

Analysis of Radiolabeled Metabolites

To analyze the radiolabeled metabolites, an HP1050 HPLC system (Agilent Technologies Inc.) was connected to a temperature controller (Waters Co.) and a Radiomatic 150TR flow scintillation analyzer (PerkinElmer). The metabolites were separated on an Adsorbosphere silica normal-phase HPLC column (250 × 4.6 mm, Prevail silica, 5 μm) using a Guard column (7.5 × 4.6 mm, Prevail silica, 5 μm) (both from Grace Davidson Discovery Sciences Inc.). The ^{14}C-labeled metabolites were identified by comparing their retention times to those of ^{14}C-labeled standard compounds (American Radiochemical Inc.).

For metabolites in the water-soluble phase, the mobile phase consisted of acetonitrile/water/ethyl alcohol/acetic acid/0.83 M sodium acetate (800:127:68:2:3 [v:v:v:v] for buffer A and 400:400:68:53:79 [v:v:v:v] for buffer B) (*12*). A linear gradient from 0% to 100% buffer B, with a slope of 5%/min, was started 15 min after initiation of the elution. The flow rate was 2.7 mL/min, and the column temperature was maintained at 45°C.

Different mobile phases were used to separate phospholipids and neutral lipids with HPLC. For phospholipids, the mobile phase consisted of acetonitrile/hexane/methanol/phosphoric acid (918:30:30:7.5, v:v:v:v) (*13*); the flow rate was 1.5 mL/min. For neutral lipids, which ^{14}C-choline does not incorporate into, the mobile phase consisted of hexane/isopropanol/acetic acid (100:2:0.02, v:v:v) (*14*); the flow rate was 2 mL/min. Nonradioactive lipid metabolites were identified by the ultraviolet detector at a wavelength of 206 nm.

Enzymatic Assay

The liver samples from HCC regions and surrounding hepatic tissues were selected for choline kinase and CCT assay through the method reported previously (*4*). For CCT assay, the freshly homogenized woodchuck liver tissues were separated into the cytosolic and microsomal fractions. The reaction mixture was divided into 2 parts; one had 1 mM oleic acid added to it and the other did not.

Molecular Species of Radiolabeled Phosphatidylcholine in Woodchuck Model of HCC

There are different phosphatidylcholine molecular species associated with phosphatidylcholine synthesis from the CDP-choline pathway and the phosphatidylethanolamine methylation pathway (*7,15*). Molecular species of phosphatidylcholine were resolved according to their degree of unsaturation by an argentation thin-layer chromatography method, which can separate phosphatidylcholine into 3 major bands (*8*). Briefly, individual eluting phosphatidylcholine peaks were collected from HPLC eluant of the lipid-soluble phase of liver tissue and spotted on the argentation thin-layer chromatography plate. The chromatographic system contained chloroform/methanol/water (50:34:7, v:v:v), with the upper band corresponding to the phosphatidylcholine species produced in the CDP-choline pathway and the lower 2 bands corresponding to the phosphatidylcholine species produced from the phosphatidylethanolamine methylation pathway. The lower band (R_f = 0.15–0.18) comigrated with the long-chain, polyunsaturated phosphatidylcholine species (6 double bonds), the middle band (R_f = 0.30–0.35) comigrated with the long-chain, polyunsaturated phosphatidylcholine species (4 double bonds), and the upper band (R_f = 0.45–0.50) comigrated with the short-chain, saturated species or unsaturated phosphatidylcholine species (2 double bonds). The radioactive bands on the thin-layer chromatography plates were detected by autoradiography with an imaging storage phosphor screen (Molecular Dynamics) and a bioimaging analyzer (Typhoon Variable Mode Imager; GE Healthcare).

Statistical Analysis

All data are expressed as mean ± SD of the mean. The data were compared using 1-way ANOVA or ANOVA on ranks when appropriate. All pairwise multiple comparison procedures used Tukey's range test, and a P value less than 0.05 was regarded as statistically significant.

RESULTS

PET/CT and Histology

A representative PET image of well-differentiated woodchuck HCCs demonstrating both ^{18}F-FDG and ^{11}C-choline uptake is shown in Figure 1. Two HCC nodules were clearly detected using choline tracer (Fig. 1B); however, these 2 nodules did not display ^{18}F-FDG uptake (Fig. 1A). The threshold for tumor detection in terms of T/L ratio was set at 1.2 (*4*), and the ^{11}C-choline detection rate for HCCs studied was in 9 of 10 woodchucks. The T/L for these 9 woodchuck HCCs was 1.89 ± 0.55, with H&E staining confirming that the 9 woodchuck HCCs were well-differentiated. The T/L of the remaining woodchuck's HCC, which could not be detected by ^{11}C-choline and from which no histology was made available, was 1.01.

HCCs are generally heterogeneous in appearance and composition. An example is illustrated in Figure 2. In this woodchuck, there were 3 distinct tumor regions. However, H&E staining showed that 1 nodule was of the compact type of HCC (Fig. 2B) whereas the other 2 nodules were the clear-cell type of HCC (Fig. 2C). In addition, the surrounding hepatic tissues (indicated by an arrow) have a noticeable level of background uptake from ^{11}C-choline (Fig. 2A). These findings suggested that between HCCs and surrounding hepatic tissues, the metabolic patterns of ^{11}C-choline are different.

Metabolite Analysis in Woodchuck Model of HCC

The uptake of ^{14}C-choline in the woodchucks is shown in Figure 3A. HCCs accumulated significantly more radioactivity than surrounding hepatic tissues, as assessed at 12 and 30 min after injection ($P < 0.05$). At 12 min after injection, approximately 70% of the radioactivity in HCCs was found in the water-soluble phase; likewise, there was also a rapid accumulation in the lipid-soluble phase (up to 25% of total radioactivity). In contrast, more than 90% of the radioactivity in surrounding hepatic tissue was found mainly in the water-soluble phase. At 30 min after injection, most radioactivity in HCCs shifted to the lipid-soluble phase, whereas that in the surrounding hepatic tissue (~75%) remained in the water-soluble phase, although some accumulation of lipid-soluble phase was also observed. Moreover, HCCs

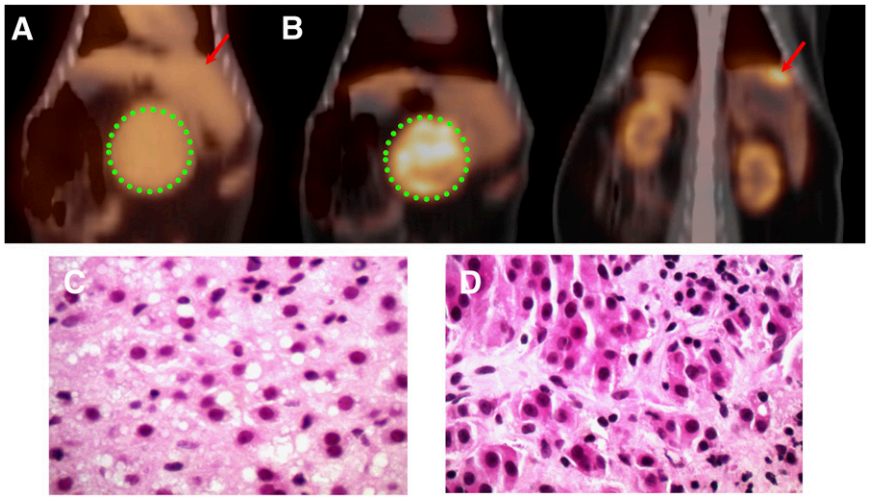

FIGURE 1. (A and B) Coronal PET/CT images of woodchuck model of HCC: ^{18}F-FDG image taken at 60 min after injection (A) and ^{11}C-choline image taken at 30 min after injection (B). Two HCC nodules are indicated by dotted rings and arrow. (C and D) H&E-stained sections (×400): surrounding hepatic tissue (C) and region within dotted rings (D).

showed a significantly higher radioactivity content in the lipid-soluble phase at 30 min after injection than did the surrounding hepatic tissues ($P < 0.05$).

HPLC analysis revealed differences in ^{14}C-choline–derived metabolites between HCCs and surrounding hepatic tissues (Fig. 3B). At 12 min after injection, the major metabolites in HCCs were phosphocholine and phosphatidylcholine, indicating a rapid transport and a high rate of ^{14}C-choline phosphorylation. In contrast, the major metabolites in surrounding hepatic tissues were betaine and, to a lesser extent, phosphocholine and free choline. The accumulation of phosphocholine in surrounding hepatic tissues after this interval suggests somewhat slower phosphorylation of choline in these tissues.

The level of ^{14}C-phosphatidylcholine was significantly higher in HCCs than in surrounding hepatic tissues at both 12 and 30 min after injection ($P < 0.05$). At the early time point (12 min), the level of ^{14}C-phosphocholine was significantly higher in HCCs than in surrounding hepatic tissues ($P < 0.05$). Furthermore, the levels of ^{14}C-betaine were significantly lower in HCCs than in surrounding hepatic tissues ($P < 0.05$) at the 12-min time point.

^{14}C-betaine was the major product in the surrounding hepatic tissues at 12 min after injection. At 30 min after injection, the decrease of ^{14}C-betaine in surrounding hepatic tissues suggests that ^{14}C-betaine might be released into the blood circulation or transfer its methyl group to methionine for subsequent incorporation into ^{14}C-phosphatidylcholine (phosphatidylethanolamine methylation pathway).

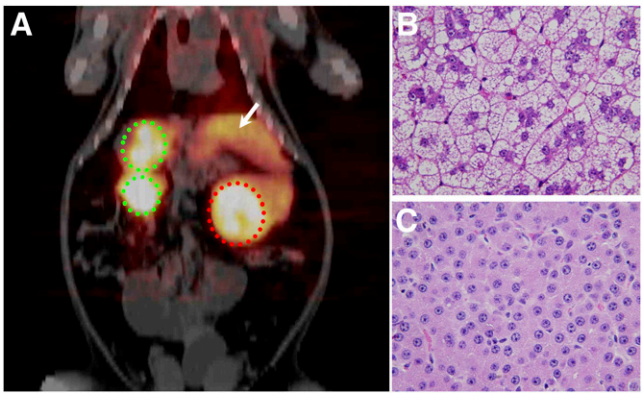

FIGURE 2. (A) Coronal PET/CT image of woodchuck model of well-differentiated HCC. Image was obtained 30 min after injection of ^{11}C-choline. Green dotted rings indicate clear cell HCC, red dotted ring indicates compact-type HCC, and arrow indicates surrounding hepatic tissue. (B and C) H&E-stained sections (×400): region within green dotted rings (B) and region within red dotted ring (C).

Choline Kinase Activity

As shown in Figure 4, the HCC regions displayed significantly increased activity of choline kinase ($P < 0.05$). However, there was no significant difference in choline kinase activity between the hepatic tissues surrounding the HCC and normal liver tissues.

Molecular Species of Radiolabeled Phosphatidylcholine in Woodchuck Model of HCC

The possible contribution of each of the pathways to the accumulation of ^{14}C-phosphatidylcholine can be assessed by comparing the degree of unsaturation of each of the phosphatidylcholine species. The proportions of radioactive species that accumulated in the 3 major fractions of phosphatidylcholine varied depending on the time after injection of ^{14}C-choline (Table 1). In HCCs, the CDP-choline pathway, as compared with the phosphatidylethanolamine methylation pathway, contributed significantly to the production of ^{14}C-phosphatidylcholine at both 12 and 30 min after injection ($P < 0.05$). However, in surrounding hepatic tissues, each pathway generated nearly even amounts of phosphatidylcholine species at the 12-min time point. At 30 min after injection, the pattern shifted, with primary production mainly from the CDP-choline pathway, hinting

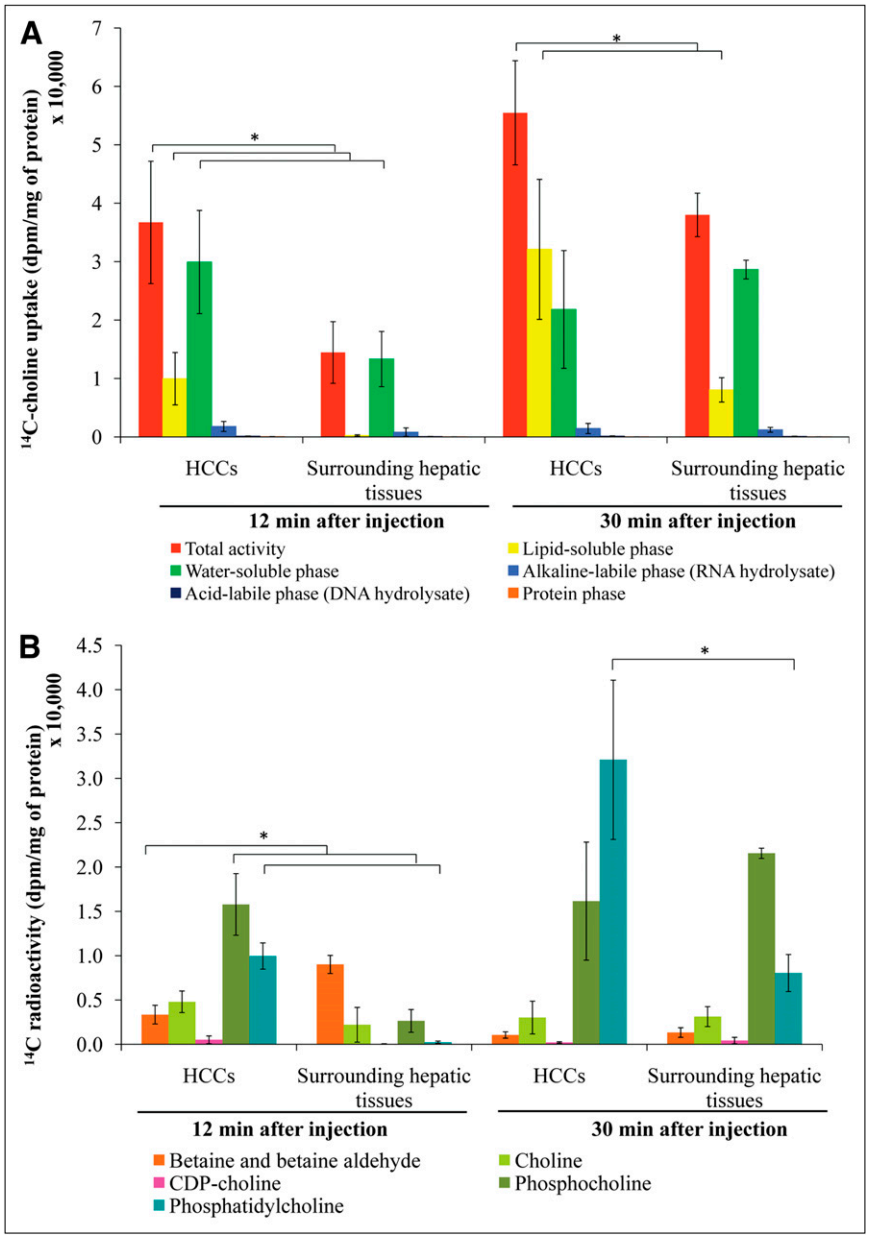

FIGURE 3. Metabolite analysis of woodchuck model of HCC using ^{14}C-choline. Distribution of ^{14}C activity between HCCs and surrounding hepatic tissues (A) and pattern of ^{14}C-choline metabolites in water- and lipid-soluble phases from woodchuck models of HCC (B). *$P < 0.05$.

at the possibility that within the surrounding hepatic tissues surrounding HCC, there is a rapid turnover rate in the phosphatidylethanolamine methylation pathway.

Our results thus suggest that in HCC, the CDP-choline pathway is the major active metabolic pathway; however, in the surrounding hepatic tissues, the phosphatidylethanolamine methylation pathway is the major active pathway at early time points, but at later time points the major contributor shifts to the CDP-choline pathway. There might be impairment along the phosphatidylethanolamine methylation pathway in HCC, as compared with surrounding hepatic tissues. Further analysis focusing on [L-methyl-^{3}H]-methionine metabolism in WCH17 cells of well-differentiated HCC also confirmed the existence of such impairment in the phosphatidylethanolamine methylation pathway in HCC (Supplemental Fig. 2).

CCT Activity

As seen in the first 12 min after injection, incorporation of ^{14}C-phosphocholine into ^{14}C-phosphatidylcholine in HCCs occurred rapidly. The amounts of tissue-extracted ^{14}C-CDP-choline in the HCCs and surrounding hepatic tissues were negligible (Fig. 3), suggesting that conversion of ^{14}C-phosphocholine to ^{14}C-CDP-choline may well be the rate-limiting step for phosphatidylcholine synthesis, which is catalyzed by key enzyme CCT.

The activity of CCT was assayed in cytosolic and micosomal fractions (Fig. 5). No significant differences in

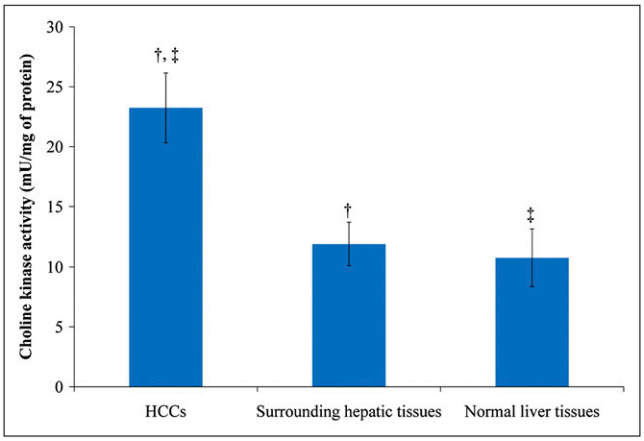

FIGURE 4. Choline kinase activity in woodchuck model of HCC. †$P < 0.05$. ‡$P < 0.05$.

microsomal CCT activity were observed between HCCs and the surrounding hepatic tissues, either with or without the addition of 1 mM oleic acid. In contrast, the cytosolic CCT activity was significantly higher in HCC than in the surrounding hepatic tissue ($P < 0.05$). In addition, the cytosolic CCT activity increased by1.4-fold in HCCs when the assay mixture contained 1 mM oleic acid and exhibited a slight increase in the surrounding hepatic tissues. Summation of the total CCT enzymatic activities from microsomes and cytosol displayed an overall increase in HCC, as compared with the surrounding hepatic tissues, both with and without 1 mM oleic acid added to the medium.

DISCUSSION

Most patients are often diagnosed with HCC at an advanced and incurable stage, and with dismal prognosis (*1*). Current diagnostic techniques include α-fetoprotein, CT, ultrasound, and MRI (*1*). Although high diagnostic yields (89%–96%) have been reported by the combined use of 2 or more of these methods, false-negative results are still common (*16*). Moreover, early detection and diagnosis remain a challenge because of the small size and minor morphologic changes of the tumors.

The diagnostic utility of ^{18}F-FDG PET is unsatisfactory for HCC, especially for well-differentiated HCC. A large amount of glucose-6-phosphatase allows FDG-6-phosphate to be reversed to ^{18}F-FDG and released from the cell, resulting in reduced accumulation of the tracer in well-differentiated and some moderately differentiated HCCs (*17*). The sensitivity of ^{18}F-FDG for HCC ranges from 50% to 70%, with an average false-negative rate of 40%–50% (*18,19*). There is an urgent need for novel PET techniques that permit earlier detection of HCC at the molecular level.

^{11}C-acetate appears to show improved sensitivity for well- and moderately differentiated HCCs (*4*), with up to 87% sensitivity (*4*). Specificity for HCC was high, with no uptake observed in other known liver tumors, such as cholangiocarcinoma, and metastatic lesions (*4*). When patients were imaged with both ^{18}F-FDG and ^{11}C-acetate, more than 85% of the HCCs showed an increased uptake for at least 1 of the tracers. However, combined use of ^{18}F-FDG and ^{11}C-acetate may pose practical issues, mostly in terms of logistics, and can hinder their translation into routine clinical use. In addition, ^{11}C-acetate has also shown increased uptake in benign tumors, such as adenoma, hemangioma, and focal nodular hyperplasia (*4*).

Recently, ^{11}C-choline and fluorocholine have been identified as metabolic probes of PET for imaging of HCC (*20*). We have demonstrated ^{11}C-choline as an appropriate PET tracer for imaging well-differentiated HCC (*4*). ^{11}C-choline PET for HCC has proven to be useful for patients with suggestive liver masses or the suggestion of HCC recurrence (*4,5*). Fluorocholine has a biodisposition and metabolic handling pattern similar to ^{11}C-choline in tumors (*20*). Fluorocholine has been shown to localize to distant metastases in the lung and bone from HCC and could also be useful for the detection of both well- and poorly differentiated HCCs (*5*). The sensitivity of fluorocholine for the

TABLE 1
Molecular Species of ^{14}C-Phosphatidylcholine Formed in Woodchuck Model of HCC

Time after injection	CDP-choline pathway (R_f = 0.45–0.50)	Phosphatidylethanolamine methylation pathway	
		R_f = 0.30–0.35	R_f = 0.15–0.18
HCCs			
12 min	80.86 ± 10.45*,† (n = 34)	11.98 ± 4.75* (n = 34)	7.30 ± 8.16† (n = 34)
30 min	95.6 ± 5.4‡ (n = 39)	4.4 ± 1.4‡ (n = 39)	ND
Surrounding hepatic tissues			
12 min	52.6 ± 11.9 (n = 6)	ND	48.4 ± 12.4 (n = 6)
30 min	100 ± 0 (n = 15)	ND	ND

*$P < 0.05$.
†$P < 0.05$.
‡$P < 0.05$.
ND = Nondetectable.
Data are percentage of total ^{14}C-phosphatidylcholine produced (n = sample numbers).

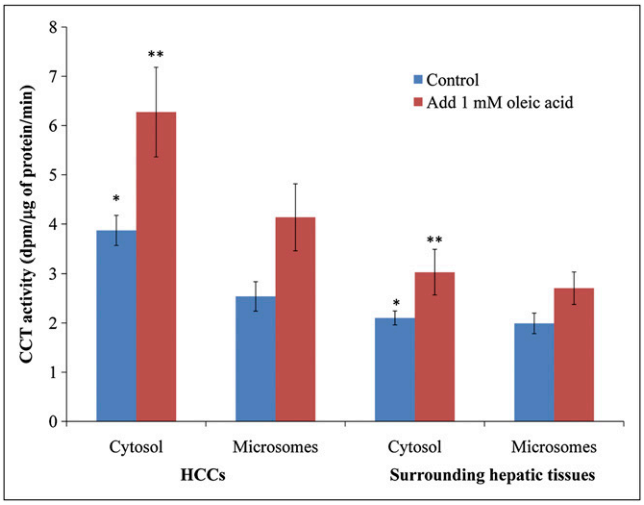

FIGURE 5. Activation of CTP:phosphocholine cytidylyltransferase by 1 mM oleic acid. *$P < 0.05$. **$P < 0.05$.

detection of HCC lesions was up to 100% in a proof-of-concept study (*5*). Furthermore, it was shown that HCC lesions as small as 9 mm could be distinguished visually and by standardized uptake value analysis on fluorocholine PET/CT (*5*). All these features may potentially make radiolabeled choline a 1-stop approach for HCC diagnosis, staging, and treatment assessment.

In the present study, we found that choline PET/CT was highly sensitive to well-differentiated HCC, with high T/L ratios for all subjects except one, for whom precancerous dysplastic nodule was suspected. The exact uptake mechanism of ^{11}C-choline in tumor cells is not well known. Several in vitro studies on the metabolism of radiolabeled choline in tumor cells have suggested that phosphocholine produced from the phosphorylation of ^{14}C-choline is the main contributor of the observed tracer accumulation (*20–23*). These studies closely agree with the results from our earlier in vitro study (*24*). In addition, a previous study on the in vivo distribution of fluorocholine in 9L-glioma–bearing Fisher rats showed that up to 99% of tumor uptake was in the water-soluble fraction after 5 min after injection and that uptake became stable by 20 min after injection (*20*). Within 20 min after injection, the lipid-soluble fraction accounted for less than 2% of total tumor uptake of fluorocholine (*20*).

However, incorporation of ^{14}C-phosphocholine into phosphatidylcholine increased in a short time span, at 30 min after injection in the present in vivo study. Oxidative metabolism of radiolabeled choline was a minor pathway in HCC. In contrast, the surrounding hepatic tissue was not particularly active in choline phosphorylation because the major radioactivity was found in ^{14}C-betaine. Moreover, by 30 min after injection, ^{14}C-phosphocholine had accumulated in the surrounding hepatic tissues only slightly. It is indicated that choline kinase is higher in regions of HCC than in the surrounding hepatic tissues. Higher choline kinase activity catalyzed the initial conversion of ^{14}C-choline to ^{14}C-phosphocholine more rapidly, followed by the conversion to ^{14}C-phosphatidylcholine to produce higher-uptake contrast in HCC regions. This high uptake observed in HCC can also be caused by the differences in choline transporter activity between HCCs and the surrounding hepatic tissues (*25*).

Cytosolic CCT is present in both active and inactive forms. In this study, cytosolic CCT activity was significantly higher in HCCs than in the surrounding hepatic tissues; the addition of 1 mM oleic acid caused an increase in the cytosolic CCT activity in HCCs. One possibility for this result is that the conversion of inactive CCT to its active form by oleic acid may be the initial event and is subsequently followed by translocation of the newly formed active CCT from cytosol to endoplasmic reticulum membranes for phosphatidylcholine synthesis (*26,27*). Another possibility could be attributed to the stability of the cytoskeleton's organization. Active CCT may be oriented along cytoskeletal elements such that the CCT complex is associated with both the endoplasmic reticulum membrane and the cytoskeleton (*28*). When this organization is disrupted, some active CCT complex may remain on the endoplasmic reticulum membrane and be released into the cytosol. As such, differences in the distribution of CCT between endoplasmic reticulum membrane and cytosol may reflect differences in the stability of the cytoskeletal organization of HCCs and normal liver cells.

In addition to the CDP-choline pathway, there also exists the phosphatidylethanolamine methylation pathway in the liver to synthesize phosphatidylcholine. Within 30 min, the major molecular species of ^{14}C-phosphatidylcholine in HCC were derived from the CDP-choline pathway. In contrast, in the surrounding hepatic tissues, phosphatidylcholine species from the phosphatidylethanolamine methylation pathway was initially predominant but reduced by 30 min. The pathophysiologic mechanism of the contribution of these 2 pathways to phosphatidylcholine species in HCC is still not fully understood. DeLong et al. (*18*) pointed out that although the contribution of choline in the CDP-choline pathway remained intact in HCC cells, the contribution of choline to the phosphatidylethanolamine methylation pathway was completely disrupted because of the lack of phosphatidylethanolamine methyltransferase activity.

Phosphatidylethanolamine-derived phosphatidylcholine cannot substitute for CDP-choline–derived phosphatidylcholine because the latter has an unknown function in DNA replication and cell division. Alternatively, phosphatidylethanolamine-derived phosphatidylcholine might, through some unknown mechanism, inhibit hepatocyte cell division (*19,29*). However, this balance may be broken in HCCs, resulting in higher activity in the CDP-choline pathway and impairment of the phosphatidylethanolamine methylation pathway.

The discrepancies of radiolabeled choline metabolite profiles observed in this study and those reported in in vitro data and data using xenograft models may be attributable to the complexity of CCT activation mechanisms and the disruption of the phosphatidylethanolamine methylation pathway in HCCs in vivo (*20,21,30*). Compared with surrounding hepatic tissues, HCC displays distinct changes in endogenous lipid components. In an examination of endogenous lipid components in the HCC nodule, the phosphatidylcholine and phosphatidylethanolamine content in C18:1ω9 (oleic acid) and C18:2ω6 (linoleic acid) had increased, whereas the contents of phosphatidylcholine and phosphatidylethanolamine in C20:4ω6 (arachidonic acid) had decreased and increased, respectively. Phosphatidylcholine and phosphatidylethanolamine contents were decreased in both C22:5ω6 (docosapentaenoic acid) and C22:6ω3 (decosahexaenoic acid) (*31*). This altered endogenous lipid profile in HCCs may create distinct microenvironments between HCCs and the surrounding hepatic tissues, resulting in the stimulation of CCT activity in HCCs (Supplemental Fig. 3). Enhanced CCT activity in HCCs could therefore facilitate the rapid synthesis of radiolabeled phosphatidylcholine synthesis in these tissues.

CONCLUSION

We have characterized the metabolism of radiolabeled choline in the woodchuck model of HCC. Despite a moderate degree of physiologic uptake, HCCs were found to have a higher uptake of radiolabeled choline than the surrounding hepatic tissues. Initially, increased radiolabeled choline uptake in HCCs is associated with the transport and phosphorylation of choline into phosphocholine. Subsequently, increased radiolabeled choline uptake reflects increased phosphatidylcholine synthesis derived from radiolabeled CDP-choline in HCCs, in contrast to the surrounding hepatic tissues in which radiolabeled choline showed extensive oxidation via the phosphatidylethanolamine methylation pathway, which contributes to a moderate degree of physiologic uptake. Future studies comparing the metabolism of radiolabeled choline between well- and poorly differentiated HCCs can be the key to determining the clinical utility of PET using radiolabeled choline for early detection, diagnosis, and staging of HCC and for evaluating response to therapy.

ACKNOWLEDGMENTS

We thank Drs. Visvanathan Chandramouli, Bill Schumann, and Ann-Marie Broome and Irene Panagopoulos for their advice and help with laboratory techniques. We also thank Dr. Jim Basilion for sharing lab resources and Dr. Steve Schomisch, Dr. Judy Zu Jin, Joseph Molter, Rachel Moore, Megan Pope, and Angie Estok for their help with animal surgery. This work was supported by an NIH/NCI grant (R01 CA095307).

REFERENCES

1. Carr BI. *Hepatocellular Cancer: Diagnosis and Treatment*. Totawa, NJ: Humana Press Inc.; 2005.
2. Gambhir SS, Czernin J, Schwimmer J, Silverman DH, Coleman RE, Phelps ME. A tabulated summary of the FDG PET literature. *J Nucl Med.* 2001;42(5, suppl):1S–93S.
3. Delbeke D, Martin WH, Sandler MP, Chapman WC, Wright JK Jr., Pinson CW. Evaluation of benign vs malignant hepatic lesions with positron emission tomography. *Arch Surg.* 1998;133:510–515.
4. Salem N, Kuang Y, Wang F, Maclennan GT, Lee Z. PET imaging of hepatocellular carcinoma with 2-deoxy-2[^{18}F]fluoro-D-glucose, 6-deoxy-6[^{18}F] fluoro-D-glucose, [(1-11)C]-acetate and [*N*-methyl-^{11}C]-choline. *Q J Nucl Med Mol Imaging.* 2009;53:144–156.
5. Talbot JN, Gutman F, Fartoux L, et al. PET/CT in patients with hepatocellular carcinoma using [^{18}F]fluorocholine: preliminary comparison with [^{18}F]FDG PET/CT. *Eur J Nucl Med Mol Imaging.* 2006;33:1285–1289.
6. Wettstein M, Weik C, Holneicher C, Haussinger D. Betaine as an osmolyte in rat liver: metabolism and cell-to-cell interactions. *Hepatology.* 1998;27:787–793.
7. DeLong CJ, Shen YJ, Thomas MJ, Cui Z. Molecular distinction of phosphatidylcholine synthesis between the CDP-choline pathway and phosphatidylethanolamine methylation pathway. *J Biol Chem.* 1999;274:29683–29688.
8. Lakher MB, Wurtman RJ. Molecular composition of the phosphatidylcholines produced by the phospholipid methylation pathway in rat brain in vivo. *Biochem J.* 1987;244:325–330.
9. Tennant BC, Toshkov IA, Peek SF, et al. Hepatocellular carcinoma in the woodchuck model of hepatitis B virus infection. *Gastroenterology.* 2004;127(5, suppl 1):S283–S293.
10. Folch J, Lees M, Sloane Stanley GH. A simple method for the isolation and purification of total lipides from animal tissues. *J Biol Chem.* 1957;226:497–509.
11. Ishiwata K, Kubota K, Murakami M, Kubota R, Senda M. A comparative study on protein incorporation of L-[methyl-^{3}H]methionine, L-[1-^{14}C]leucine and L-2-[^{18}F]fluorotyrosine in tumor bearing mice. *Nucl Med Biol.* 1993;20:895–899.
12. Liscovitch M, Freese A, Blusztajn JK, Wurtman RJ. High-performance liquid chromatography of water-soluble choline metabolites. *Anal Biochem.* 1985; 151:182–187.
13. Arduini A, Peschechera A, Dottori S, Sciarroni AF, Serafini F, Calvani M. High performance liquid chromatography of long-chain acylcarnitine and phospholipids in fatty acid turnover studies. *J Lipid Res.* 1996;37:684–689.
14. Hamilton JG, Comai K. Separation of neutral lipids and free fatty acids by high-performance liquid chromatography using low wavelength ultraviolet detection. *J Lipid Res.* 1984;25:1142–1148.
15. LeKim D, Betzing H, Stoffel W. Studies in vivo and in vitro on the methylation of phosphatidyl-*N,N*-dimethylethanolamine to phosphatidylcholine in rat liver. *Hoppe Seylers Z Physiol Chem.* 1973;354:437–444.
16. Gao H, Lu Q, Liu X, et al. Application of ^{1}H NMR-based metabonomics in the study of metabolic profiling of human hepatocellular carcinoma and liver cirrhosis. *Cancer Sci.* 2009;100:782–785.
17. Gharib AM, Thomasson D, Li KC. Molecular imaging of hepatocellular carcinoma. *Gastroenterology.* 2004;127(5, suppl 1):S153–S158.
18. DeLong CJ, Hicks AM, Cui Z. Disruption of choline methyl group donation for phosphatidylethanolamine methylation in hepatocarcinoma cells. *J Biol Chem.* 2002;277:17217–17225.
19. Vance DE, Houweling M, Lee M, Cui Z. Phosphatidylethanolamine methylation and hepatoma cell growth. *Anticancer Res.* 1996;16(3B):1413–1416.
20. Bansal A, Shuyan W, Hara T, Harris RA, Degrado TR. Biodisposition and metabolism of [18F]fluorocholine in 9L glioma cells and 9L glioma-bearing fisher rats. *Eur J Nucl Med Mol Imaging.* 2008;35:1192–1203.
21. Yoshimoto M, Waki A, Obata A, Furukawa T, Yonekura Y, Fujibayashi Y. Radiolabeled choline as a proliferation marker: comparison with radiolabeled acetate. *Nucl Med Biol.* 2004;31:859–865.
22. Hara T, Bansal A, DeGrado TR. Choline transporter as a novel target for molecular imaging of cancer. *Mol Imaging.* 2006;5:498–509.
23. Al-Saeedi F, Welch AE, Smith TA. [methyl-^{3}H]Choline incorporation into MCF7 tumour cells: correlation with proliferation. *Eur J Nucl Med Mol Imaging.* 2005;32:660–667.
24. Kuang Y, Salem N, Corn DJ, et al. Transport and metabolism of radiolabeled choline in hepatocellular carcinoma. *Mol Pharm.* September 21, 2010 [Epub ahead of print].
25. Kwee SA, DeGrado TR, Talbot JN, Gutman F, Coel MN. Cancer imaging with fluorine-18-labeled choline derivatives. *Semin Nucl Med.* 2007;37:420–428.
26. Weinhold PA, Rounsifer ME, Charles L, Feldman DA. Characterization of cytosolic forms of CTP: choline-phosphate cytidylyltransferase in lung, isolated

alveolar type II cells, A549 cell and Hep G2 cells. *Biochim Biophys Acta.* 1989;1006:299–310.
27. Feldman DA, Rounsifer ME, Charles L, Weinhold PA. CTP:phosphocholine cytidylyltransferase in rat lung: relationship between cytosolic and membrane forms. *Biochim Biophys Acta.* 1990;1045:49–57.
28. Rao RH, Mansbach CM II. Purification and partial characterization of intestinal acid lipase. *Biochim Biophys Acta.* 1990;1046:19–26.
29. Cui Z, Houweling M, Vance DE. Expression of phosphatidylethanolamine *N*-methyltransferase-2 in McArdle-RH7777 hepatoma cells inhibits the CDP-choline pathway for phosphatidylcholine biosynthesis via decreased gene expression of CTP:phosphocholine cytidylyltransferase. *Biochem J.* 1995;312:939–945.
30. DeGrado TR, Coleman RE, Wang S, et al. Synthesis and evaluation of ^{18}F-labeled choline as an oncologic tracer for positron emission tomography: initial findings in prostate cancer. *Cancer Res.* 2001;61:110–117.
31. Abel S, Smuts CM, de Villiers C, Gelderblom WC. Changes in essential fatty acid patterns associated with normal liver regeneration and the progression of hepatocyte nodules in rat hepatocarcinogenesis. *Carcinogenesis.* 2001;22: 795–804.

Errata

In the article "^{18}F-FDG PET/CT for the Prediction and Detection of Local Recurrence After Radiofrequency Ablation of Malignant Lung Lesions," by Singnurkar et al. (*J Nucl Med.* 2010;51:1833–1840), Table 2 contained an error. The corrected table appears below. The authors regret the error.

TABLE 2
Local Recurrence According to Pattern of Uptake on Post-RFA Scan

Pattern	Recurrence	Nonrecurrence
Favorable		
Diffuse	5	10
Heterogeneous	0	1
Rim	3	6
Rim plus focal, not corresponding	1	2
Unfavorable		
Focal	2	1
Rim plus focal, corresponding	8	1

In the article "Serotonin Transporters in Dopamine Transporter Imaging: A Head-to-Head Comparison of Dopamine Transporter SPECT Radioligands ^{123}I-FP-CIT and ^{123}I-PE2I," by Ziebell et al. (*J Nucl Med.* 2010;51:1885–1891), the third and fourth sentences of the abstract contain errors and should read as follows: "In this study, we compared the SPECT radioligands ^{123}I-2-β-carbomethoxy-3β-(4-iodophenyl)-*N*-(3-fluoropropyl)nortropane (^{123}I-FP-CIT) and ^{123}I-*N*-(3-iodoprop-2E-enyl)-2-β-carbomethoxy-3β-(4-methylphenyl)nortropane (^{123}I-PE2I), which has a 10-fold higher selectivity than ^{123}I-FP-CIT for DAT versus SERT." We regret the errors.